Journal of Research in Pharmacy

Research Article

www.jrespharm.com

Treatment of glioblastoma by photodynamic therapy with the aid of synthesized silver nanoparticles by green chemistry from *Citrus aurantium*

Ömer ERDOĞAN [1]*, Mürüvvet ABBAK [2], Gülen Melike DEMİRBOLAT [3], Mehran AKSEL [4], Salih PAŞA [5], Gizem DÖNMEZ YALÇIN [6], Özge ÇEVİK [1]

1 Department of Biochemistry, School of Medicine, Aydın Adnan Menderes University, Aydın, Turkey.
2 Scientific Technology Research and Application Centre, Aydın Adnan Menderes University, Aydın, Turkey.
3 Department of Pharmaceutical Technology, Faculty of Pharmacy, Acıbadem University, İstanbul, Turkey.
4 Department of Biophysics, School of Medicine, Aydın Adnan Menderes University, Aydın, Turkey.
5 Department of Science, Faculty of Education, Afyon Kocatepe University, Afyonkarahisar, Turkey.
6 Department of Medical Biology, School of Medicine, Aydın Adnan Menderes University, Aydın, Turkey.

* Corresponding Author. E-mail: ozge.cevik@adu.edu.tr (O.C.); Tel. +90-256-218 20 00.

Received: 07 June 2021 / Revised: 21 August 2021/ Accepted: 26 August 2021

ABSTRACT: Blood brain barrier is very important to provide treatment locally for the treatment of glioblastoma. The use of nanoparticles has shown promise for glioblastoma treatments in recent years. In this study, the effect of the combined treatment of silver nanoparticles (AgNPs) synthesized from *Citrus aurantium* with photodynamic therapy (PDT) was investigated on U87 glioblastoma cells. AgNPs were characterized by FTIR, zeta potential and SEM images. U87 cells were treated with AgNPs (10 µg/mL) and/or PDT (0.5 mJ/cm^2) at 24 h. Cells antiproliferative effect, migration levels, colony formation capability, Bax and Bcl-2 protein/gene expression, and caspase-3 activity levels as apoptotic markers were measured. AgNPs size were found at 141±3 nm and 18.1±1.3 mV as zeta potential. It was found that cell proliferation, migration and Bcl-2 protein/gene levels decreased, and Bax protein/gene levels and caspase-3 activity increased via AgNPs and PDT combined treatment. As a result, nanoparticles synthesized from *Citrus aurantium* are eco-friendly and their size can cross the blood brain barrier. If AgNPs is used with PDT, it may be a new therapy for clinically treatment of glioblastoma in the future.

KEYWORDS: Glioblastoma; photodynamic therapy; silver nanoparticles; green chemistry; *Citrus aurantium*.

1. INTRODUCTION

Glioblastoma (GBM) is the most common and aggressive type of brain tumors that derives from glia cells. 20-30 % of primary brain tumors are classified under glioblastoma and observed mostly at 45-70 years of age. Glioblastomas are characterized by a high mortality rate together with intratumorally heterogeneity and the invasive growth potential of the tumor [1]. Unfortunately, less than 7% of patients survive five years after diagnosis of GBM [2]. Glioblastomas rarely metastasize outside the brain and the cranium inhibits their growth inside the brain. Therefore, glioblastoma cells create space for their growth by killing neurons around them via excitotoxicity, which is the excess accumulation of glutamate in synaptic cleft [3]. Glioblastomas are characterized by dysregulation of major signaling pathways including growth, proliferation, survival, and apoptosis. Therefore, glioblastoma biology has been widely studied identifying molecular pathways which underly the disease mechanism such as p53, pRB (tumor suppressor retinoblastoma), PI3K-PTEN-Akt-mTOR, RAS/MAPK, STAT3 and ZIP4 signaling pathways, together with related miRNAs, cancer stem cells, extracellular matrix elements and other cancer-related cellular processes [4]. Although a better understanding of the molecular mechanisms underlying glioblastomas has been achieved recently, the treatment of glioblastomas unfortunately lacks efficacy. The current regimen followed for glioblastoma patients include surgical resection, followed by chemotherapy and/or radiation therapy. Currently, the average survival rate

How to cite this article: Erdoğan O, Abbak M, Demirbolat GM, Aksel M, Paşa S, Dönmez Yalçın G, Çevik Ö. Treatment of glioblastoma by photodynamic therapy with the aid of synthesized silver nanoparticles by green chemistry from *Citrus aurantium*. J Res Pharm. 2021; 25(5): 641-652.

ISSN: 2630-6344

https://dx.doi.org/10.29228/jrp.56

for GBM is less than 15 months [4]. Therefore, in order to improve the patient outcomes, exploring and developing different ways of glioblastoma treatments is urgently needed.

Nanoparticle systems have come forward in the recent years. These molecules are candidates for the glioblastoma therapy and drug development since they have the potency to be led to the target and the size to be able to pass the blood brain barrier. The nanoparticles are mostly used as a drug delivery system in the therapy for glioblastoma [5]. It is possible to use solely nanoparticles in the glioblastoma therapy [6]. Especially, silver nanoparticles (AgNPs) are able to show an anti-cancer effect in some cancer types alone [7]. AgNPs may localize in perinuclear membrane and endolysosomal membranes after being endocytosed into the cell [8]. It is also known that silver nanoparticles induce apoptosis via changing the mitochondrial membrane [9]. Photodynamic therapies applied with nanoparticles accelerate these changes in the mitochondria. Photodynamic therapy is a noninvasive system where light at a specific wavelength is sent onto nanoparticles so that electron release and an increase in cellular reactive oxygen species (ROS) levels occur [10, 11]. The increased cellular ROS levels, which show effect on the change of energy levels in mitochondria, induce cell death in cancer [12, 13]. In this study, we synthesized silver nanoparticles with green chemistry method using *Citrus aurantium* and induced with PDT in order to examine its potential in the glioblastoma therapy.

2. RESULTS AND DISCUSSION

2.1. Synthesis and characterization of AgNPs

AgNPs can be synthesized by three methods such as physical, chemical, and green synthesis methods. When the advantages and disadvantages of these methods are compared, green synthesis seems to be the optimal method. Expensive equipments, high temperature and high pressure are needed for the physical method. Toxic chemicals which are dangerous for the nature and the living things are used for the chemical method. On the other hand, green synthesis is known to be a cheaper and an environment-friendly method. The plants, bacteria, fungi and algs are used for the synthesis of nanoparticles [14, 15]. Especially, in the method of green synthesis, the plants and the plant extracts are preferred [16]. Due to the rich bioactive ingredients that they contain, plant metal atoms can be oxidized in plant extracts and therefore they are mostly preferred for the nanoparticle synthesis. These bioactive ingredients can bind to the surface of metal oxides during the process of synthesis and this leads to the gain of anti-bacterial and anti-cancer properties by the metal oxides [17, 18].

In the synthesis of AgNPs via green chemistry, after adding any extract to $AgNO_3$ solution, the color gradually turns to dark brown [19-21]. This color change is an indicator of the synthesis of silver nanoparticles and it is due to the excitation of the surface plasmon on silver nanoparticles. Biogenic silver nanoparticles give a sharp peak at 430±20 nm in the UV spectrum because of plasmon resonance vibration. Forough and Farhadi [22] was found that the UV spectrum absorbance of silver nanoparticles synthesized with *acanthe phylum bracteatum* extract was 425 nm. In addition, biogenic silver nanoparticles synthesized by Singh et al [23] gave the sharp peak in the UV spectrum at 440 nm. In our study, figure 1a shows UV-Vis spectra recorded from *Citrus aurantium* peel extracts and different silver nitrate concentrations. The UV spectrum of AgNPs synthesized by us shows the maximum wavelength in the range of 350-570 nm and intense spectrum at 435nm. The narrow peaks are indicated the synthesis of small- sized nanoparticles (Fig 1a).

Silver nanoparticles contain bioactive components found in plant extracts, which are used as reducing agents during the synthesis. Functional group analysis on to silver nanoparticles resulting from these bioactive components is verified by FTIR [24-27]. In our study, the FTIR spectrum of silver nanoparticles synthesized with *Citrus aurantium* peel aqueous extract is given in figure 1b. Stretching vibrations 671 cm^{-1} can also be attributed to the reduction of Ag+ to Ag. Disappearance of the most of the functional groups such as carbonyl and hydroxyl may be due to the bio-reduction during the Ag-NP production. The other bands at the 2881, 2362, 1600, 1413, 1139,1095, 1012 cm^{-1} come from organic residues of *Citrus aurantium* L on to AgNPs and the bonds represented by these bands are given in the Table 1.

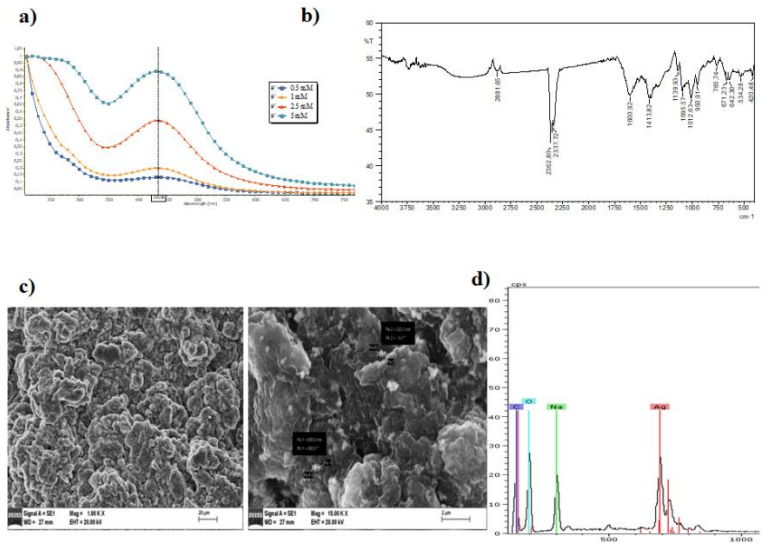

Figure 1. Characterization of synthesized AgNPs from *Citrus aurantium* a) UV spectrum, b) FT-IR spectrum, c) SEM images at different magnitudes and d) Energy-dispersive X-ray spectroscopy spectrum of AgNPs.

Table 1. Identification of the vibrations of AgNPs.

Wavenumber cm^{-1}	Possible Bond	Possible Functional Group
2881	C-H stretch	Aliphatics
2362		Atmospheric carbondioxide
1600	C-C strech (in ring)	Aromatics
1413	-CH2- bending	Aliphatics
1139	C-N stretch	Aromatic amines
1095	C-N stretch	Aliphatic amines
1012	C-O stretch	Ether

In this study, the synthesis of AgNPs was achieved by using the peels of *Citrus aurantium* L., which is commonly known as bitter orange and usually utilized as a flavoring and acidifying agent for food. The chemical composition includes vitamins, minerals, phenolic compounds, terpenoids, and flavonoids [28]. The fact that *C. aurantium* can be used in nanoparticle synthesis due to its rich ingredients was shown with numerous studies [29]. In a recent study, AgNPs with 60.5 nm size was synthesized from *C. aurantium* and was shown to have an anti-fungal property against *Candida albicans* [29]. In our study, we examined the combined effect of AgNPs synthesized from *C. aurantium* and PDT in U87 cells. Our study is the first in literature showing the anticancer activity of AgNPs synthesized from *C. aurantium*. Size analysis of nanoparticles to be used in biological studies is very important. Because it must be in nano-size in order to pass through the cell and organelle membrane. Morphological analysis of silver nanoparticles is generally examined by scanning electron microscopy. Spherical, ellipsoidal, flake type, rocky and irregular shapes can be seen in SEM micrographs. Silver nanoparticles sometimes tend to agglomerate. SEM technique was used to identify the morphological structure and size of AgNPs synthesized from *Citrus aurantium* (Fig 1c). Surface morphology of biogenic AgNPs also seems agglomerated. It has irregularly shaped particles with various sizes. The diameter of broken particles from agglomerated AgNPs has measured between 133 nm and 200 nm in SEM micrograph [30, 31]. AgNPs were seen as clusters and showed a uniform distribution. Particle sizes of AgNPs were found at 141±3 nm size with relatively homogenous distribution (polydispersity index: 0.355±0.028). Just like in our study, silver nanoparticles synthesized by with *Coffee arabica* extract also showed a tendency to agglomeration [32].

Nanoparticles display electrostatic interaction and show affinity to various receptors, glycoproteins, anionic phospholipids and glycosaminoglycans on the cell membrane. Nanoparticles are able to enter into the cells due to their charges [33]. The engulfment of negatively charged nanoparticles via endocytosis is achieved since they can bind to the cationic sites [34]. The membranes of glial cells are heavily populated with anionic phospholipids [35] and it was shown that anionic phospholipids and glycosaminoglycans are increased in

cancerous cells [19]. Zeta potential is an important parameter in measuring the stability of a nanoparticle in aqueous solutions, its surface charge is an indication for the entrance of the particles to the cell. The AGNPs that we obtained in this study have zeta charges as -18.1±1.3 mV and their sizes are 141±3 nm and they enter into the cell at physiological pH.

Figure 1d shows the energy dispersive analysis by X-rays (EDAX) spectrum of AgNPs synthesized by *Citrus aurantium* extract and it is observed that sodium ions apart from the presence of carbon and oxygen originating from the bioorganic component of the extract. 25.17 % has obtained by EDX analysis that reveals the abundance of Ag-NPs.

2.2. Cell viability and nuclear deformation with AgNPs and/or PDT therapy

In the literature, AgNPs were combined with chemotherapeutic agents in various glioblastoma therapies. In a recent study, it was shown in GBM02 glioblastoma cells that silver/silver chloride nanoparticles (Ag/AgCl-NPs) were combined with a chemotherapeutic agent temozolomide, which led to a decrease in astrocyte proliferation [36]. In another study, in chicken embryo chorioallantoic membrane model of U87 cells, AgNPs treatment reduced tumor growth with an increase in Caspase-3 and Caspase-9 levels [37]. In a study with U251 human glioblastoma cells, AgNPs were shown to enter the cell via endocytosis and may increase stress and hence lead to a dysfunction in calcium exchange and elevate cell proliferation at increasing concentrations [7]. In apoptotic cells, calcium exchange is dysfunctional and as a result cytochrome c is induced and apoptotic proteins are released from mitochondria [38].

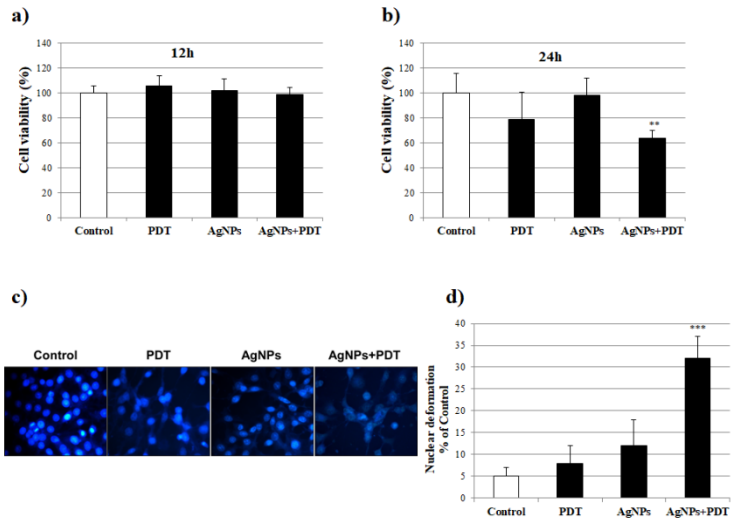

Figure 2. a) AgNPs (10 µg/mL) and/or PDT (0.5 mJ/cm²) on the cell viability in U87 glioblastoma cells for 12h (a) and 24 h (b). c) Cell nuclear morphology and deformation after treatment AgNPs and/or PDT treatment U87 cell lines for 24 h using Hoechst 33342 staining. d) Ratio of nuclear deformation in U87 cells with treated of AgNPs and/or PDT for 24h (**p<0.01 compare to control).

In our study, U87 cells were treated with AgNPs and/or PDT for 12 and 24 hours and the cell viability was measured. The cell viability did not show a significant difference with 12 hour treatments of AgNPs and/or PDT (Fig 2a). However, the cell viability with 24 hour treatment of AgNPs and PDT showed a decrease compared to control cells (**p<0.01, Fig 2b). Nuclear deformation and membrane integrity were analyzed using Hoechst 33342 staining in 24-hour AgNPs and/or PDT treated cells. When the nuclear morphology and cell interactions were analyzed with microscopy, the deformation was found to be increased with AgNPs or PDT treatment, although not statistically significant. Similarly, the cells which were both treated with AgNPs and PDT, the nuclear deformation was significantly increased compared to control cells (**p<0.001, Fig 2c-d). The combined treatment of cells with AgNPs and PDT induced a change in the morphology of the cell and its nucleus. As a result, this change prevented the cell proliferation and cell-to-cell interaction.

2.3. Cell migration and colony formation with AgNPs and/or PDT therapy

The effect of a 24-hour treatment with AgNPs and/or PDT on cell migration in U87 cells was examined with wound healing assay. The migration ability of the cells was decreased with PDT application, although

not significantly. Similarly, AgNPs treatment reduced the cell migration significantly (**p<0.01, Fig 3a-b). The combined treatment of AgNPs and PDT prevented the cell migration significantly (**p<0.01). Colony formation was analyzed as the proliferation capacity in a determined number of cells for 7 days with AgNPs and/or PDT treatment. Colony formation did not show a difference in U87 cells with PDT treatment only; however, colony formation was reduced in AgNPs and AgNPs+PDT treated U87 cells compared to controls significantly (*p<0.05, Fig 3c-d).

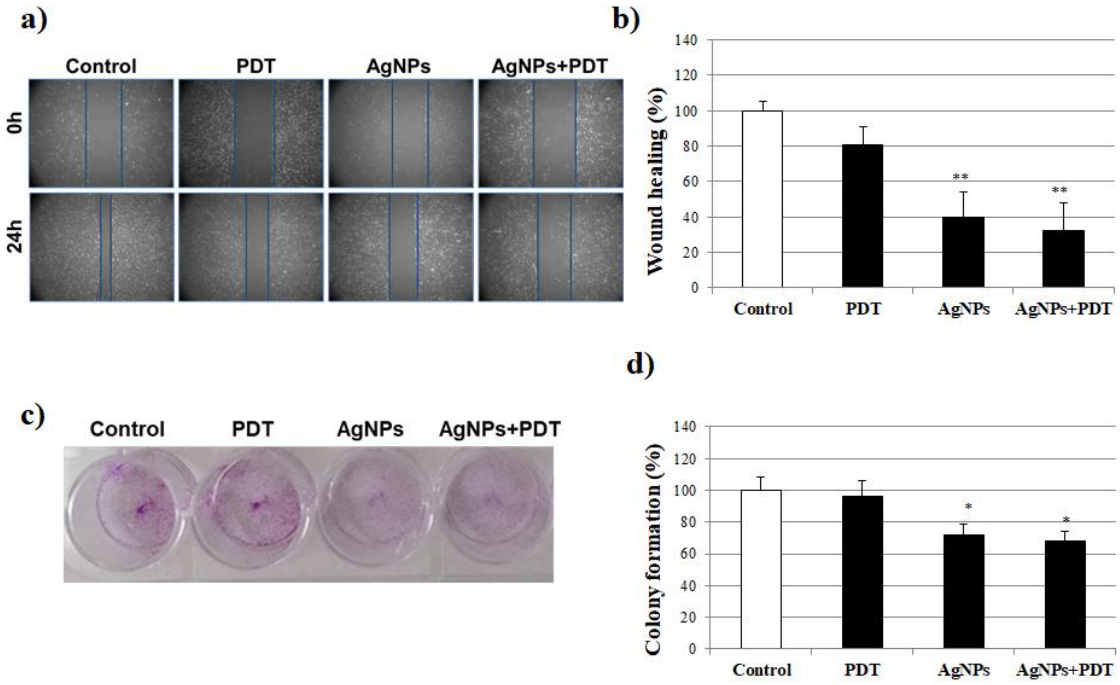

Figure 3. a) AgNPs (10 µg/mL) and/or PDT (0.5 mJ/cm²) on wound healing in U87 cancer cells b) The rate of wound closure was calculated differences of cells filling the scratched area c) Colony formation stained with crystal violet d) Ratio of cell formation in U87 cells with treated of AgNPs and/or PDT for 24h (**p<0.01 compare to control).

2.4. The change in apoptosis with AgNPs and/or PDT therapy

In cancer cells, PDT is one of the methods used for increasing the anti-cancer effects of nanoparticles [39]. Especially in PDT, it is crucial to use nontoxic compounds which obtain cytotoxic properties when exposed to light at a certain wavelength [40]. Nanoparticles are advantageous for this matter since they can easily penetrate the cells. When PDT is applied to nanoparticles, they can transfer their energy to cellular oxygen and harm the cellular constituents and also induce singlet oxygen and increase reactive oxygen species (ROS) resulting in the elevation of anticancer activity [41, 42]. As a result of all these studies, apoptotic death is started in cancer cells. In our previous study, we showed that AgNPs synthesized from the Cynara scolymus leaf extracts combined with PDT therapy increased ROS levels and apoptosis and reduced proliferation in breast cancer cells [12]. There are many studies in the literature regarding the PDT applications in glioblastoma therapies [43, 44]. It was shown in T98-G, U87-MG, U343 glioblastoma cells and NIH-3T3 fibroblast cells that low dose temozolomide (TMZ) chemotherapeutic agent combined with PDT therapy reduced cell proliferation in cancer cells and did not display toxicity in healthy cells [45]. In vivo studies showed that tumor proliferation decreased, apoptosis increased and hence survival increased in rats with glioblastoma in which single dose ionizing radiation was applied with AgNPs [46]. In in vitro and in vivo studies conducted with glioblastoma-astrocytoma epithelial-like cell line (U87MG) cells, the combination therapy including AgNPs, chemotherapeutic agent alisertib and radiotherapy reduced the tumor growth [47]. In our study with U87 cells, we observed that the combined therapy with AgNPs and PDT resulted in a decrease in cell proliferation and increase in apoptosis via regulating the gene and protein expressions of apoptotic markers and the membrane structure.

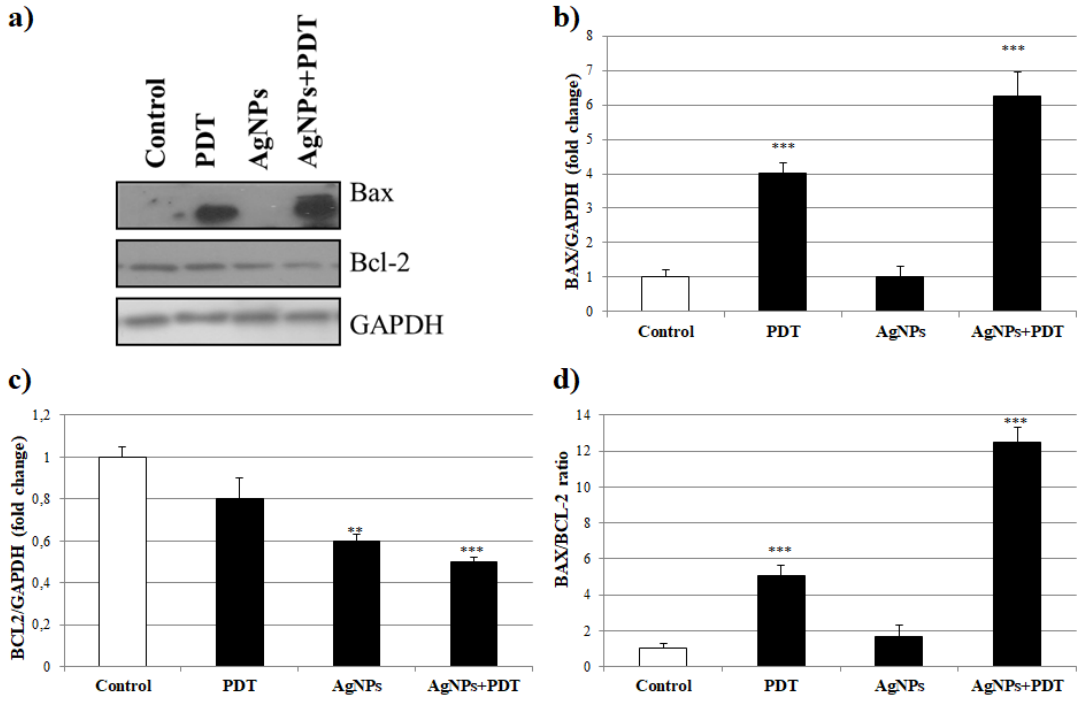

Figure 4. a) Western bands of Bax and Bcl-2 proteins analysis apoptotic proteins in AgNPs (10 µg/mL) and/or PDT (0.5 mJ/cm²) for 24h treatment in U87 cells. Western blot densitometry analysis of b) Bax, c) Bcl-2 and d) ratio of Bax/Bcl-2 protein expression levels in U87 cells. Each protein band was normalized to the intensity of GAPDH used. (**p<0.01, ***p<0.001, compare to control cells).

Apoptosis can be triggered with a variety of ways in the cell. After some mitochondrial changes in the cell, an intrinsic apoptotic pathway can be preferred by the cell with the differences in Bax or Bcl-2 protein expressions, which are apoptotic markers. In this study, the protein (Fig 4) or gene (Fig 5) expressions of Bax and Bcl-2 were examined after AgNPs and/or PDT treatment in U87 cells. The expression of Bax, a proapoptotic protein, was significantly increased with PDT treatment only (***p<0.001). While the sole treatment of AgNPs did not lead to a change in Bax protein expression, AgNPs+PDT led to a significant increase in Bax expression compared to controls (***p<0.001, Fig 4 b). The expression of Bcl-2, an anti-apoptotic protein, did not show a significant change with PDT treatment only. However, the Bcl-2 protein expression was significantly decreased with AgNPs (**p<0.01) and AgNPs+PDT treatments (***p<0.001) (Fig 4c). Bax/Bcl-2 rate is a well-known indicator of apoptosis inducement. Therefore, it was shown that the AgNPs+PDT treatment triggers apoptosis 12.5 more compared to the control group in U87 cells (***p<0.001, Fig 4d). When Bax gene expression levels were compared among the groups, it showed a significant increase in PDT (***p<0.001), AgNPs (*p<0.05) and AgNPs+PDT (***p<0.001) treatment groups compared to control (Fig 5 a). While Bcl-2 gene expression did not show a significant difference in sole treatments of PDT or AgNPs treatments, it is reduced significantly with AgNPs+PDT treatments compared to controls (***p<0.01, Fig 5 b). When the rates of Bax/Bcl-2 gene expression levels were compared, significant increases were observed in PDT (***p<0.001), AgNPs (*p<0.05) and AgNPs+PDT (***p<0.001, Fig 5c) treatment groups. Changes in caspase-3 activity, indicative of apoptosis and indicating its initiation, were also detected (Fig 5d). Caspase-3 activity levels were compared, significant increases were observed in PDT (*p<0.05), and AgNPs+PDT (***p<0.001) treatment groups. There was no significant change observed in the group treated with AgNPs alone in U87 cells.

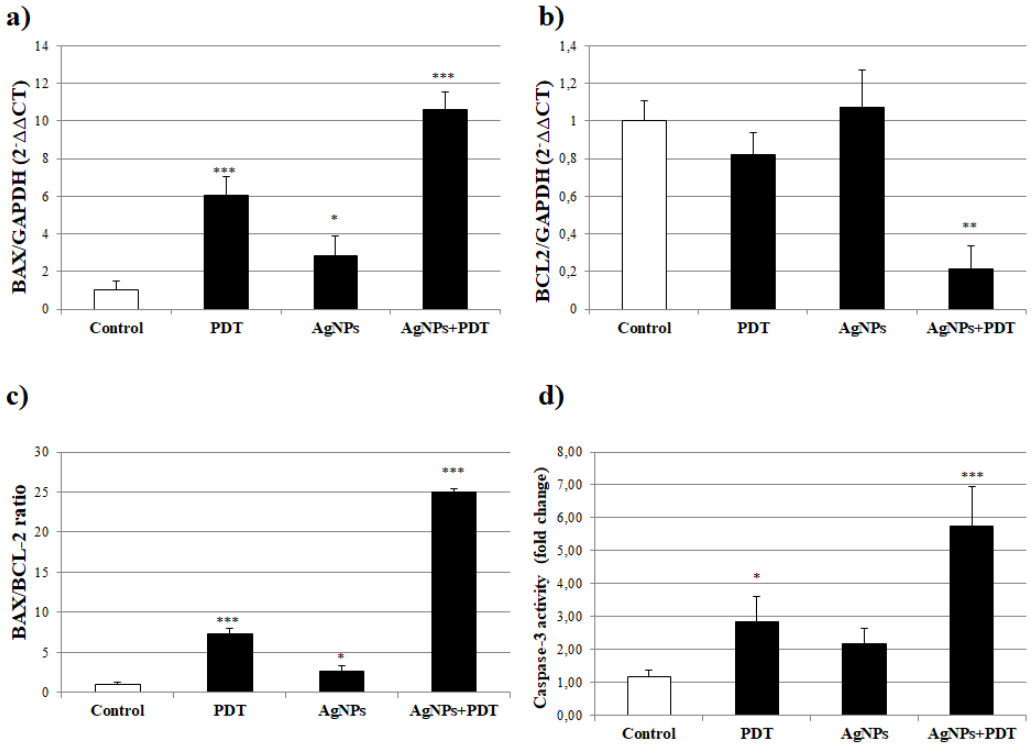

Figure 5. Gene expression of Bax and Bcl-2 in AgNPs (10 µg/mL) and/or PDT (0.5 mJ/cm²) for 24h treatment in U87 cells. a) Bax, b) Bcl-2 and c) ratio of Bax/Bcl-2 gene expression levels in U87 cells. For normalization, GAPDH was used as housekeeping gene d) Caspase-3 activity levels AgNPs (10 µg/mL) and/or PDT (0.5 mJ/cm²) for 24h treatment in U87 cells. (*p<0.05, **p<0.01, ***p<0.001, compare to control cells)

3. CONCLUSION

Since glioblastoma is one of the most aggressive and high mortality tumor types, scientists are trying to develop new treatment methods. Silver nanoparticles can be used alone or in combination with any other agent in the treatment of glioblastoma. In this study, an effective treatment is developed on U87 glioblastoma cells by combining photodynamic therapy and silver nanoparticles synthesized with the green method. With photodynamic therapy, the effectiveness of silver nanoparticles on glioblastoma is increased by creating more oxidative stress. In addition, chemical synthesis, which requires the use of toxic materials, was not preferred in the synthesis of silver nanoparticles. Instead of chemical synthesis, silver nanoparticles were synthesized by using *Citrus aurantium* peel aqueous extract via green synthesis, which is a more nature and live friendly method.

In summary, AgNPs synthesized using the peels of *Citrus aurantium* can be used in a combination with PDT treatment as an effective therapy with low toxicity due to their small size and ability to cross the blood brain barrier with their charges.

4. MATERIALS AND METHODS

4.1. The preparation of *Citrus aurantium* fruit peel extract

Citrus aurantium grown in the Aydin region were collected in three location (37°51'16"N 27°51'42"E; 37°51'12"N 27°51'04"E; 37°51'36"N 27°51'20"E). Prof. Dr. Osman TUGAY from the Department of Pharmaceutical Botany, Faculty of Pharmacy, Konya Selcuk University/Turkey has identified voucher specimens. The fruit peel of the *Citrus aurantium* were removed and washed 3 times with deionized water. Peels were passed through the kitchen robot to separate small pieces. 200 g *Citrus aurantium* leaves and 400 mL deionized water were added to one liter erlenmeyer. The mixture was heated in a magnetic heater at 100 °C for 2 hours. The mixture was filtered through Whatman filter paper (Grade 1) to give an extract [48]. Experimental details were presented in Figure 6.

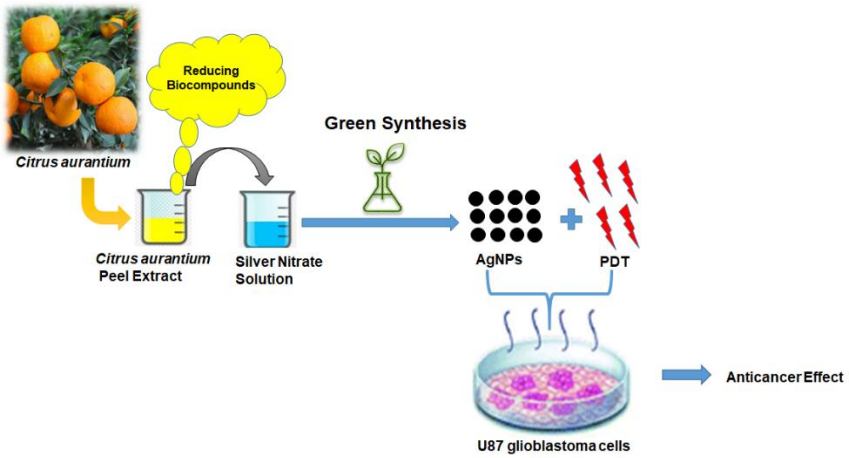

Figure 6. Experimental design for green synthesis and biological process.

4.2. The synthesis of silver oxide nanoparticles

20 mL of silver nitrate (10 mM) solution was added in a 100 mL beaker. 20 mL of *Citrus aurantium* extract was added dropwise to this mixture. It was placed in the ultrasonic bath for waves at a 35 kHz frequency at room temperature for 30 minutes (Sonorex Bandelin RK100, Germany). Then it was subjected to 360 W microwave irradiation for 5 min. The mixture was centrifuged for 20 minutes at 4000 rpm. To remove organic residues, the pellet was washed 5 times with ethanol. The powder form of nanoparticles obtained by lyophilization and was kept at room temperature for further study [49, 50].

4.3. Characterization of silver oxide nanoparticles

The formation of Ag nanoparticles was observed by Ultraviolet-visible (UV-Vis) spectrophometer (Thermo Scientific Multiscan Spectrum 1500) with a range of 200-800 nm. The functional groups on to synthesized AgNPs were validated with Fourier-transform infrared (FTIR) spectroscopy using in the range of 400-4000 cm^{-1} (Shimadzu IR 8000). The surface morphology and the structural properties of AgNPs were characterized by SEM (LEO 1430 VP). Elemental compositions were analyzed by EDX (LEO 1430 VP). Particle size, distribution and zeta potentials of nanoparticles were determined using Zeta Sizer-Nano ZS (Malvern Instruments, England). An aliquot of nanoparticles was diluted with pure water, then sonicated for 10 minutes before the measurements.

4.4. Preparation of cell culture

U87 human glioblastoma cancer cells were cultured and maintained in Dulbecco's Modified Eagle Medium (DMEM) containing 10% fetal bovine serum (FBS) and supplemented with 100 U/mL^{-1} penicillin and 100 µg/mL streptomycin. The cultures were incubated at 37 °C in a humidified atmosphere with 5% CO_2.

4.5. PDT treatment for cell line

For experiments, the cells were irradiated with 0.5 mJ/cm2 light intensity of the light from a solar simulator (Abet Technologies, USA) and midOpt SP785-105 infrared dichroic block filter and LP590-105 red long pass filter. AgNPs were incubated 10 µg/mL concentration during 4 hours in U87 cells and irradiated with PDT. After the treatment, the cells were cultured for 24 h and then prepared for different analyses [51].

4.6. Antiproliferative assay

The effect of AgNPs with/without PDT on glioblastoma cancer cell viability was determined using a tetrazolium-based microplate assay with MTT (Vybrant, Life Technologies). Briefly, the U87 cells were seeded into a 96-well plate at a density of 1×10^4 cells/well. After incubating the cells for 24 h, the AgNPs at (10 µg/mL) were added and incubated for 12 h and 24 h. After that, the culture medium was discarded and the wells were washed with PBS twice, followed by the addition of 20 µL MTT dye (0.5 mg/mL) each well. The cells were incubated for another 4 h at 37°C. After removing all the culture medium, 150 µL DMSO was added per well.

The percentage of cell viability was measured on a microplate reader (Biotek Co., USA) at the wavelength of 490 nm. The cell inhibitory rate was calculated using the Graphpad Prism programme [52].

4.7. Colony formation assay

AgNPs with/without PDT treated cells were seeded in to a 24 well plate at a density of 400 cells/well. Cell were cultured at 37°C for 7 days. The medium was changed every 3 days. At the end of incubation, cells were fixed with absolute ethanol for 20 sec, stained with 0.5% crystal violet for 15 min and washed with PBS until clear. For cell counting, 1% of SDS was added and absorbance was measured at 470 nm by ELISA reader [53].

4.8. Hoechst 33342 staining

Hoechst 33342 double staining in cultured U87 cells was measured to detect apoptosis after the treatment of AgNPs with/without PDT. Cells ($1x10^5$) were cultured in a six-well plate and treated with different concentrations of AgNPs then eight hours incubated with PDT exposed cells. Control cells were maintained without adding AgNPs. After a 24-h incubation, cells were washed with phosphate buffered saline (PBS, pH 7.4) and then fixed with 70% ice-cold ethanol for 10 min. The fixed cells were washed with PBS and stained with Hoechst 33342 (1 µg/mL) for 10 min. After discard of the excess dye by washing with PBS repeatedly, images of cells were captured under a fluorescence microscope (Zeiss Axiovert, Germany) [12].

4.9. Wound healing assay

U87 cells ($1x10^5$ cells/well) were seeded into a 12 well culture plate and were allowed to grow overnight to reach confluence in DMEM media. Cells were treated AgNPs with/without PDT. The monolayer was then scratched with a pipette tip, washed with PBS twice to remove floating cells, and treated with control media. After incubation period of 24 h, the cells migrated into the scratched area were photographed under a phase-contrast inverted microscope. The distance that cells had migrated into the cell-free space was measured by Image J software. The width of each migrated area was used to calculate the relative proportion wounded at time zero [53].

4.10. Bax and Bcl-2 gene expression with qPCR

Bax and Bcl-2 gene expression as marker mediators of apoptosis were determined using quantitative real- time polymerase chain reaction (Q- PCR). Gene expressions by Q- PCR measurement were performed using Power SYBR Green PCR Master Mix (ABI- 4368577). RNA from U87cells were isolated by using PureLink RNA Mini Kit (Invitrogen, K1560- 02) kit. DNA was synthesized from the isolated RNA and was used for measurement of Bax and Bcl-2 gene expression by using special primer pairs for the human Bax and Bcl-2 genes. The following primer sequences were used Bax F:5'-GCCCTTTTGCTTCAGGGTTT-3', R: 5'-TCCAATGTCCAGCCCATGAT-3' and Bcl-2 F: 5'-GACAGAAGATCATGCCGTCC-3', R: 5'-GGTACCAATGGCACTTCAAG-3'. Gene expression analysis was normalized to the housekeeping gene GAPDH and performed using the comparative Ct ($2^{-\Delta\Delta Ct}$) for fold change [54].

4.11. Bax and Bcl-2 protein expression with western blotting

After treatment of AgNPs with/without PDT for 24 h, total cellular proteins were prepared using RIPA lysis buffer (included protease inhibitor cocktail) from U87 cells. The protein concentrations were established by bicinchoninic acid assay. Equal amount of protein was separated by 12% polyacrylamide gels and then transferred onto PVDF membranes. The membranes were blocked with 2.5% BSA at 4°C overnight and then incubated with specific primary antibodies (Bax and Bcl-2, Santa Cruz). After washing with TBST (containing 0.1% Tween 20) 3 times, the membranes were incubated with the corresponding HRP-conjugated secondary antibodies in TBST at 37°C for 1 h. The protein GAPDH was used as a housekeeping control for normalization. Finally, the expression levels of proteins were visualized and analyzed using ImageJ software [55].

4.12. Caspase-3 activity

After treatment, cells were collected and lysed with lysis buffer. Caspase- 3 activity assay was performed with caspase- 3 activity assay kit according to the manufacturer's instructions (APT131; Millipore).

Acknowledgements: This work was supported by Adnan Menderes University Research Grant (ADU-MARL-18001 and TPF-19037). The analysis was conducted by the Adnan Menderes University Science and Technology Research Center (ADU-BILTEM), of which is gratefully acknowledged.

Author contributions: Concept – O.E., O.C.; Design – O.E., G.D.Y., M.A., O.C.; Supervision – O.C.; Resources – G.D.Y, O.C.; Materials –O.E, G.M.D., M.A., S.P.; Data Collection and/or Processing – O.E., M.A., M.A., S.P.; Analysis and/or Interpretation – O.E., G.M.D., S.P.; Literature Search – O.E., G.D.Y, O.C.; Writing – O.E., G.D.Y, O.C.; Critical Reviews – O.E., G.M.D., M.A., M.A., S.P ,G.D.Y., O.C.

Conflict of interest statement: The authors declared no conflict of interest.

REFERENCES

[1] Obara-Michlewska M, Szeliga M. Targeting glutamine addiction in gliomas. Cancers. 2020; 12(2): 310. [CrossRef]

[2] Ostrom QT, Cioffi G, Gittleman H, Patil N, Waite K, Kruchko C, et al. CBTRUS statistical report: primary brain and other central nervous system tumors diagnosed in the United States in 2012–2016. Neuro-oncology. 2019; 21(Supplement_5): v1-v100.

[3] Cuddapah VA, Robel S, Watkins S, Sontheimer H. A neurocentric perspective on glioma invasion. Nat Rev Neurosci. 2014; 15(7): 455-465. [CrossRef]

[4] Mao H, LeBrun DG, Yang J, Zhu VF, Li M. Deregulated signaling pathways in glioblastoma multiforme: molecular mechanisms and therapeutic targets. Cancer Invest. 2012; 30(1): 48-56. [CrossRef]

[5] Alphandéry E. Nano-therapies for glioblastoma treatment. Cancers. 2020; 12(1): 242. [CrossRef]

[6] Liang P, Shi H, Zhu W, Gui Q, Xu Y, Meng J, et al. Silver nanoparticles enhance the sensitivity of temozolomide on human glioma cells. Oncotarget. 2017; 8(5): 7533. [CrossRef]

[7] Asharani P, Hande MP, Valiyaveettil S. Anti-proliferative activity of silver nanoparticles. BMC Cell Biol. 2009; 10(1): 1-14. [CrossRef]

[8] Greulich C, Diendorf J, Simon T, Eggeler G, Epple M, Köller M. Uptake and intracellular distribution of silver nanoparticles in human mesenchymal stem cells. Acta Biomater. 2011; 7(1) :347-354. [CrossRef]

[9] Kim S, Choi JE, Choi J, Chung K-H, Park K, Yi J, et al. Oxidative stress-dependent toxicity of silver nanoparticles in human hepatoma cells. Toxicol in vitro. 2009; 23(6): 1076-1084. [CrossRef]

[10] Huang Z. A review of progress in clinical photodynamic therapy. Technol Cancer Res Treat. 2005; 4(3): 283-293. [CrossRef]

[11] Yi G, Hong SH, Son J, Yoo J, Park C, Choi Y, et al. Recent advances in nanoparticle carriers for photodynamic therapy. Quant Imaging Med Surg. 2018; 8(4): 433. [CrossRef]

[12] Erdogan O, Abbak M, Demirbolat GM, Birtekocak F, Aksel M, Pasa S, et al. Green synthesis of silver nanoparticles via Cynara scolymus leaf extracts: The characterization, anticancer potential with photodynamic therapy in MCF7 cells. PLoS One. 2019; 14(6): e0216496. [CrossRef]

[13] Lucky SS, Soo KC, Zhang Y. Nanoparticles in photodynamic therapy. Chem Rev. 2015; 115(4): 1990-2042. [CrossRef]

[14] Chen J, Liu X, Wang C, Yin S-S, Li X-L, Hu W-J, et al. Nitric oxide ameliorates zinc oxide nanoparticles-induced phytotoxicity in rice seedlings. J. Hazard. Mater. 2015; 297: 173-182. [CrossRef]

[15] Agarwal H, Kumar SV, Rajeshkumar S. A review on green synthesis of zinc oxide nanoparticles–An eco-friendly approach. J Resource-Efficient Technologies. 2017; 3(4): 406-413. [CrossRef]

[16] Shanmuganathan R, MubarakAli D, Prabakar D, Muthukumar H, Thajuddin N, Kumar SS, et al. An enhancement of antimicrobial efficacy of biogenic and ceftriaxone-conjugated silver nanoparticles: green approach. Environ Sci Pollut Res. 2018; 25(11): 10362-10370. [CrossRef]

[17] Ibrahim HM. Green synthesis and characterization of silver nanoparticles using banana peel extract and their antimicrobial activity against representative microorganisms. J Radiat Res Appl Sci. 2015; 8(3): 265-275. [CrossRef]

[18] Kaviya S, Santhanalakshmi J, Viswanathan B, Muthumary J, Srinivasan. Biosynthesis of silver nanoparticles using Citrus sinensis peel extract and its antibacterial activity. Spectrochim Acta A Mol Biomol Spectrosc. 2011; 79(3): 594-598. [CrossRef]

[19] Zhang T, Chan C-F, Lan R, Li H, Mak N-K, Wong W-K, et al. Porphyrin-based ytterbium complexes targeting anionic phospholipid membranes as selective biomarkers for cancer cell imaging. Chem Commun. 2013; 49(65): 7252-7254. [CrossRef]

[20] Nadagouda MN, Varma RS. Green synthesis of silver and palladium nanoparticles at room temperature using coffee and tea extract. Green Chem. 2008; 10(8): 859-862. [CrossRef]

[21] Fatimah I, Aftrid ZHVI. Characteristics and antibacterial activity of green synthesized silver nanoparticles using red spinach (Amaranthus Tricolor L.) leaf extract. Green Chem Let Rev. 2019; 12(1): 25-30. [CrossRef]

[22] Forough M, Fahadi K. Biological and green synthesis of silver nanoparticles. Turk J Eng Environ Sci. 2011; 34(4): 281-287. [CrossRef]

[23] Singh V, Shrivastava A, Wahi N. Biosynthesis of silver nanoparticles by plants crude extracts and their characterization using UV, XRD, TEM and EDX. Afr J Biotechnol. 2015; 14(33): 2554-2567. [CrossRef]

[24] Majumdar R, Bag BG, Maity N. Acacia nilotica (Babool) leaf extract mediated size-controlled rapid synthesis of gold nanoparticles and study of its catalytic activity. Int Nano Let. 2013; 3(1): 1-6. [CrossRef]

[25] Li S, Shen Y, Xie A, Yu X, Qiu L, Zhang L, et al. Green synthesis of silver nanoparticles using Capsicum annuum L. extract. Green Chem. 2007; 9(8): 852-858. [CrossRef]

[26] Vigneshwaran N, Ashtaputre N, Varadarajan P, Nachane R, Paralikar K, Balasubramanya R. Biological synthesis of silver nanoparticles using the fungus Aspergillus flavus. Materials letters. 2007; 61(6): 1413-1418. [CrossRef]

[27] Jain D, Daima HK, Kachhwaha S, Kothari S. Synthesis of plant-mediated silver nanoparticles using papaya fruit extract and evaluation of their anti microbial activities. Dig J Nanomater Biostructures. 2009; 4(3): 557-63.

[28] Suntar I, Khan H, Patel S, Celano R, Rastrelli L. An overview on Citrus aurantium L.: Its functions as food ingredient and therapeutic agent. Oxid Med Cell. Longev. 2018;2018. [CrossRef]

[29] Albahadly ZK, Albahrani RM, Hamza AM. Silver Nanoparticles Synthesized from Citrus aurantium L. & Citrus sinensis L. leaves and Evaluation the Antimicrobial Activity. J Glob Pharma Technol. 2009; 11(3): 71-75. [CrossRef]

[30] Sondi I, Salopek-Sondi B. Silver nanoparticles as antimicrobial agent: a case study on E. coli as a model for Gram-negative bacteria. J Colloid Interface Sci. 2004; 275(1): 177-182. [CrossRef]

[31] Jeevan P, Ramya K, Rena AE. Extracellular biosynthesis of silver nanoparticles by culture supernatant of Pseudomonas aeruginosa. Indian J Biotechnol. 2012; 11: 72-76. [CrossRef]

[32] Dhand V, Soumya L, Bharadwaj S, Chakra S, Bhatt D, Sreedhar B. Green synthesis of silver nanoparticles using Coffea arabica seed extract and its antibacterial activity. J Mater Sci Eng C. 2016; 58: 36-43. [CrossRef]

[33] Honary S, Zahir F. Effect of zeta potential on the properties of nano-drug delivery systems-a review (Part 2). Trop J Pharm Res. 2013; 12(2): 265-273. [CrossRef]

[34] Patil S, Sandberg A, Heckert E, Self W, Seal S. Protein adsorption and cellular uptake of cerium oxide nanoparticles as a function of zeta potential. Biomaterials. 2007; 28(31): 4600-4607. [CrossRef]

[35] Chrast R, Saher G, Nave K, Verheijen M. Lipid metabolism in myelinating glial cells: lessons from human inherited disorders and mouse models. J Lipid Res. 2011; 52: 419. [CrossRef]

[36] Eugenio M, Campanati L, Müller N, Romão LF, de Souza J, Alves-Leon S, et al. Silver/silver chloride nanoparticles inhibit the proliferation of human glioblastoma cells. Cytotechnology. 2018; 70(6): 1607-1618. [CrossRef]

[37] Urbańska K, Pająk B, Orzechowski A, Sokołowska J, Grodzik M, Sawosz E, et al. The effect of silver nanoparticles (AgNPs) on proliferation and apoptosis of in ovo cultured glioblastoma multiforme (GBM) cells. Nanoscale Res. Lett. 2015; 10(1): 1-11. [CrossRef]

[38] Liang W-Z, Chou C-T, Chang H-T, Cheng J-S, Kuo D-H, Ko K-C, et al. The mechanism of honokiol-induced intracellular Ca2+ rises and apoptosis in human glioblastoma cells. Chem Biol Interact. 2014; 221: 13-23. [CrossRef]

[39] Bechet D, Couleaud P, Frochot C, Viriot M-L, Guillemin F, Barberi-Heyob M. Nanoparticles as vehicles for delivery of photodynamic therapy agents. Trends Biotechnol. 2008; 26(11): 612-621. [CrossRef]

[40] Sivasubramanian M, Chuang YC, Lo L-W. Evolution of nanoparticle-mediated photodynamic therapy: from superficial to deep-seated cancers. Molecules. 2019; 24(3): 520. [CrossRef]

[41] Castano AP, Demidova TN, Hamblin MR. Mechanisms in photodynamic therapy: part one—photosensitizers, photochemistry and cellular localization. Photodiagnosis Photodyn Ther. 2004; 1(4): 279-293. [CrossRef]

[42] Price M, Reiners JJ, Santiago AM, Kessel D. Monitoring singlet oxygen and hydroxyl radical formation with fluorescent probes during photodynamic therapy. Photochem. Photobiol. 2009; 85(5): 1177-1181. [CrossRef]

[43] Abliz E, Collins JE, Bell H, Tata D. Novel applications of diagnostic X-rays in activating a clinical photodynamic drug: Photofrin II through X-ray induced visible luminescence from" rare-earth" formulated particles. J X-Ray Sci Technol. 2011; 19(4): 521-530. [CrossRef]

[44] de Melo MT, Piva HL, Tedesco AC. Design of new protein drug delivery system (PDDS) with photoactive compounds as a potential application in the treatment of glioblastoma brain cancer. J Mater Sci Eng C. 2020; 110: 110638. [CrossRef]

[45] Pellosi DS, Paula LB, de Melo MT, Tedesco AC. Targeted and synergic glioblastoma treatment: multifunctional nanoparticles delivering verteporfin as adjuvant therapy for temozolomide chemotherapy. Mol Pharm. 2019; 16(3): 1009-1024. [CrossRef]

[46] Liu P, Huang Z, Chen Z, Xu R, Wu H, Zang F, et al. Silver nanoparticles: a novel radiation sensitizer for glioma? Nanoscale. 2013; 5(23): 11829-11836. [CrossRef]

[47] Locatelli E, Naddaka M, Uboldi C, Loudos G, Fragogeorgi E, Molinari V, et al. Targeted delivery of silver nanoparticles and alisertib: in vitro and in vivo synergistic effect against glioblastoma. Nanomedicine. 2014; 9(6): 839-49. [CrossRef]

[48] Ganapathi Rao K, Ashok C, Venkateswara Rao K, Shilpa Chakra C, Akshaykranth A. Eco-friendly synthesis of MgO nanoparticles from orange fruit waste. Int J Adv Res Phys Sci. 2015; 2: 1-6.

[49] Joseph S, Mathew B. Microwave-assisted green synthesis of silver nanoparticles and the study on catalytic activity in the degradation of dyes. J Mol Liq. 2015; 204: 184-191. [CrossRef]

[50] Haris M, Kumar A, Ahmad A, Abuzinadah MF, Basheikh M, Khan SA, et al. Microwave-assisted green synthesis and antimicrobial activity of silver nanoparticles derived from a supercritical carbon dioxide extract of the fresh aerial parts of Phyllanthus niruri L. Trop J Pharm Res. 2017; 16(12): 2967-2976. [CrossRef]

[51] Aksel M, Bozkurt-Girit O, Bilgin MD. Pheophorbide a-mediated sonodynamic, photodynamic and sonophotodynamic therapies against prostate cancer. Photodiagnosis Photodyn Ther. 2020; 31: 101909. [CrossRef]

[52] Türk S, Tok F, Erdoğan Ö, Çevik Ö, Tok TT, Koçyiğit-Kaymakçıoğlu B, et al. Synthesis, anticancer evaluation and in silico ADMET studies on urea/thiourea derivatives from gabapentin. Phosphorus Sulfur Silicon Relat Elem. 2020: 1-7. [CrossRef]

[53] Cevik O, Turut FA, Acidereli H, Yildirim S. Cyclosporine-A induces apoptosis in human prostate cancer cells PC3 and DU145 via downregulation of COX-2 and upregulation of TGFβ. Turk J Biochem. 2018; 44(1): 47-54. [CrossRef]

[54] Cevik O, Acidereli H, Turut FA, Yildirim S, Acilan C. Cabazitaxel exhibits more favorable molecular changes compared to other taxanes in androgen- independent prostate cancer cells. J Biochem Mol Toxicol. 2020; 34(9): e22542. [CrossRef]

[55] Cevik O, Li D, Baljinnyam E, Manvar D, Pimenta EM, Waris G, et al. Interferon regulatory factor 5 (IRF5) suppresses hepatitis C virus (HCV) replication and HCV-associated hepatocellular carcinoma. J Biol Chem. 2017; 292(52): 21676-21689. [CrossRef]